Chemical analysis of HfO_2/Si (100) film systems exposed to NH_3 thermal processing

Patrick S. Lysaght,[a] Joel Barnett, and Gennadi I. Bersuker
Front End Process Division, SEMATECH, 2706 Montopolis Drive, Austin, Texas 78741-6499

Joseph C. Woicik and Daniel A. Fischer
National Institute of Standards and Technology, Gaithersburg, Maryland 20899

Brendan Foran[b]
Physical Characterization Laboratory, Advanced Technology Development Facility, 2706 Montopolis Drive, Austin, Texas 78741-6499

Hsing-Huang Tseng and Raj Jammy
Front End Process Division, SEMATECH, 2706 Montopolis Drive, Austin, Texas 78741-6499

(Received 13 April 2006; accepted 1 November 2006; published online 17 January 2007)

Nitrogen incorporation in HfO_2/SiO_2 films utilized as high-k gate dielectric layers in advanced metal-oxide-semiconductor field effect transistors has been investigated. Thin HfO_2 blanket films deposited by atomic layer deposition on either SiO_2 or NH_3 treated Si (100) substrates have been subjected to NH_3 and N_2 anneal processing. Several high resolution techniques including electron microscopy with electron energy loss spectra, grazing incidence x-ray diffraction, and synchrotron x-ray photoelectron spectroscopy have been utilized to elucidate chemical composition and crystalline structure differences between samples annealed in NH_3 and N_2 ambients as a function of temperature. Depth profiling of core level binding energy spectra has been obtained by using variable kinetic energy x-ray photoelectron spectroscopy with tunable photon energy. An "interface effect" characterized by a shift of the Si^{4+} feature to lower binding energy at the HfO_2/SiO_2 interface has been detected in the Si 1s spectra; however, no corresponding chemical state change has been observed in the Hf 4f spectra acquired over a broad range of electron take-off angles and surface sensitivities. The Si 2p spectra indicate Si–N bond formation beneath the HfO_2 layer in the samples exposed to NH_3 anneal. The NH_3 anneal ambient is shown to produce a metastable Hf–N bond component corresponding to temperature driven dissociation kinetics. These findings are consistent with elemental profiles across the $HfO_2/Si(100)$ interface determined by electron energy loss spectroscopy measurements. X-ray diffraction measurements on similarly treated films identify the structural changes resulting from N incorporation into the HfO_2 films. © *2007 American Institute of Physics*. [DOI: 10.1063/1.2422746]

I. INTRODUCTION

Metal-oxide-semiconductor field effect transistor (MOSFET) device scaling has driven an industry wide effort to replace the conventional transistor gate dielectric layer, SiO_2, with a high permittivity (high-k) material since physically thicker high-k films offer lower leakage current characteristics for equivalent SiO_2 capacitance.[1,2] This initiative has given rise to extensive evaluation of Hf based oxide thin films as one of the most promising candidates for alternative gate dielectrics. However, intrinsic properties of hafnia, HfO_2, do not satisfy all the requirements for gate dielectric thin films, particularly crystallization temperature, defect density, and ion diffusivity among others. Therefore, various attempts have been undertaken to modify the hafnia structure to address these issues.

Several groups have reported beneficial results from N incorporation in HfO_2 including improved thermal stability of the dielectric material,[3] reduction of boron penetration,[4] reduction of gate leakage current, increase in dielectric constant, and suppression of the onset of crystallization.[5] It has been shown previously that the chemical composition of a thin SiO_2 interface between HfO_2 and the Si substrate may be modified by exposure to NH_3 with significant consequences for carrier mobility and equivalent oxide thickness (EOT) scaling.[6,7] In this study, we investigate N incorporation into the HfO_2 gate stack by means of pre- and post-high-k-deposition thermal treatments in N_2 and NH_3 ambients to identify physical characteristics of N incorporation corresponding to enhanced performance. Evaluating the change in microstructure and bonding configurations as a function of anneal temperature and ambient will contribute to the evolution of more precise models of NH_3 dissociation and the corresponding chemical explanations describing nitrogen-for-oxygen exchange mechanisms. Elucidating the role of N as a diffusion inhibitor and identifying its influence on the local coordination of Hf and associated crystallization kinetics of HfO_2 thin films is critical to the understanding and control of fabrication processes integral to device performance optimization.

[a]Electronic mail: pat.lysaght@sematech.org
[b]Present address: The Aerospace Corporation, 2350 E. El Segundo Blvd., El Segundo, CA 90245.

0021-8979/2007/101(2)/024105/9/$23.00 © 2007 American Institute of Physics

Downloaded 27 May 2008 to 129.6.180.72. Redistribution subject to AIP license or copyright; see http://jap.aip.org/jap/copyright.jsp

TABLE I. Sample set indicating NH_3 exposure both pre- and post-HfO_2-deposition and the resultant N dose measured by nuclear reaction analysis using $^{14}N(d,\alpha)^{12}C$.

Sample	Interface	Pre-deposition anneal	High-*k* deposition	Post-deposition anneal	STEM Interface (nm)	STEM HfO_2 thick (nm)	[N] (1×10^{15} cm^{-2})
A	ISSG 2 nm	None	HfO_2	NH_3/PDA	1.9–2.0	3.2–3.3	3.57
B	HF-last	NH_3/pre-DA	HfO_2	None	1.3–1.4	2.9–3.0	2.14
C	HF-last	NH_3/per-DA	HfO_2	NH_3/PDA	1.2–1.3	3.2–3.3	5.91

A. Nitrogen incorporation

Incorporation of nitrogen into Hf based oxide films is expected to reduce the diffusion rate of all elemental species in the bulk medium, thereby elevating the onset of crystallization temperature, since crystallization is a diffusion-limited phase transition where the rate depends on the Gibbs free-energy difference of the phases.[8,9] It is also well known that the concentration and position of N near the channel region of transistors must be well controlled to circumvent consequences of reduced electron mobility and N-induced band-gap narrowing.[10] Hafnium oxynitride, HfO_xN_y, may be formed by nitridation of the oxide or oxidation of the nitride. Adding N reduces the Hf coordination with oxygen by displacing O with N of slightly lower electronegativity. However, when oxidizing the nitride, one concern centers on the effective transformation of conductive HfN into the dielectric while avoiding formation of electrically nanostructured heterogeneous (ENH) HfO_xN_y compositions where conductive nanoscale inclusions are embedded in a dielectric matrix.[11–13]

The resultant position of N in Hf based oxide gate dielectric film systems is also a strong function of the nitridation methodology, i.e., N plasma, N-bearing precursor chemistry, N_2^+ implantation, and anneal ambient (NH_3, NO, N_2O, N_2) exposure. During thermal processing, N may exchange for O via displacement of lattice oxygen ions in the evolving grain structures of HfO_2 films and/or incorporate in lattice interstitials as excess N. Plasma nitridation has been shown to incorporate molecular nitrogen, N_2, as interstitials in SiO_xN_y films.[14,15] In the case of plasma nitridation, ionized N_2^+ species are likely to incorporate into the film. No atomic dissociation of N_2 is expected, which is consistent with the fact that nitrogen is known to be an inert anneal ambient for oxides at 900 °C.[16] In contrast to the N_2 molecule, the atomic N interstitial has no affinity for a second electron and is also stable as a positive ion.

N incorporation resulting from ammonia and its reactions has been the subject of numerous studies during the past two decades, involving various experimental techniques utilized to elucidate the adsorption geometries, vibrational interactions, electronic structures, and reaction energies. Initial reports suggested that NH_3 underwent a complete dissociation on the Si (100) surface at low temperature (−180 °C) and that chemisorbed H would saturate the dangling bonds, while N occupied the surface sites.[17,18] Recently, however, advanced techniques have fostered a consensus that NH_3 molecules adsorb molecularly as well as dissociatively below room temperature with NH_2 and H as the only dissociative products.[19,20] NH_2 is stable up to ~325 °C and above this temperature NH_2 either recombines with H to produce NH_3 or dissociates to H and N, followed by H_2 liberation and N incorporation.[21,22] Specific to the HfO_2/SiO_2 film system, it has been calculated by Gavartin *et al.*[23] that during postdeposition anneal (PDA) of HfO_2 at 700 °C, NH_3 dissociation consists of NH_2^- and a proton, H^+. Further dissociation of the NH_2^- molecule may lead to the formation of NH species where NH^0 is stable while NH^- is unstable, suggesting that the likely final products of the NH_3 PDA process are NH_2^-, NH^0, H^+, and H^-.

B. Characterization techniques

HfO_2 gate dielectric thin films (3 nm thick) have been atomic layer deposited (ALD) via tetrakis(ethylmethylamino)hafnium precursor with ozone [(TEMAHf)+O_3] on chemically prepared *p*-type Si (100) substrates and exposed to a 700 °C PDA processing for 60 s in either NH_3 or N_2 ambient at 30 Torr. By comparing films exposed to the NH_3 PDA process with otherwise identical films exposed to N_2 PDA, the effect of N incorporation (NH_3) may be decoupled from that of the thermal cycle (N_2 itself is not reactive to HfO_2). The impact of N treatments on the electrical performance was evaluated based on EOT and mobility values collected on complementary metal-oxide semiconductor (CMOS) transistors fabricated with the gate dielectrics described above. The N dose (atoms/cm^2) in the bulk films exposed to NH_3 has been quantified by nuclear reaction analysis (NRA). Additional duplicate samples exposed to a subsequent higher temperature rapid thermal anneal (RTA) in N_2 ambient have been characterized by grazing incidence x-ray diffraction (GIXRD) for comparative crystallographic phase identification as a function of ambient and temperature. Synchrotron x-ray photoelectron spectroscopy (XPS) has been utilized to determine N 1*s* core level binding energy variations associated with both Hf–N and Si–N bond formation. High-angle annular dark field scanning transmission electron microscopy (HAADF-STEM) in combination with electron energy loss spectroscopy (EELS) was used to produce atomic-number sensitive "Z-contrast" images and elemental profiles of silicon, oxygen, nitrogen, and hafnium to illustrate chemical intensity gradients as a function of position across the interfacial regions of the $HfO_2/SiO_2/Si$ film systems in cross section.

II. EXPERIMENT

Table I indicates the three basic NH_3 processes corresponding to the primary three-sample set under evaluation.

Downloaded 27 May 2008 to 129.6.180.72. Redistribution subject to AIP license or copyright; see http://jap.aip.org/jap/copyright.jsp

Sample A consists of a Si surface that had an *in situ* steam generated (ISSG) 2 nm thick thermal SiO_2 layer grown on it prior to HfO_2 deposition, and samples B and C consist of Si surfaces that were cleaned with an HF-last chemical sequence (H-terminated Si) and then annealed in NH_3 at 700 °C for 15 s (predeposition anneal) prior to HfO_2 deposition. A 3 nm thick ALD HfO_2 film was then deposited on each substrate. After HfO_2 deposition, samples A and C received a 700 °C anneal for 60 s in NH_3 (postdeposition anneal), while sample B was characterized as deposited. The nitrogen dose indicated for each sample in Table I has been quantified by NRA utilizing a Van de Graaf accelerator sensitive to ^{14}N from the $^{14}N(d,\alpha)^{12}C$ reaction at 1.1 MeV incident deuteron energy with a detection limit of $\sim 5 \times 10^{13}$ atoms/cm^2.

In order to evaluate physical parameter variations including material intermixing corresponding to chemical processing, phase contrast high resolution transmission electron microscopy (HRTEM) and *Z*-contrast HAADF-STEM with EELS elemental chemical profile scans were performed on the three-sample set. STEM, EELS, and energy dispersive x-ray spectroscopy (EDXS) data were recorded at 300 keV using focused electron probes of ~0.3 nm full width at half maximum (FWHM). A detailed explanation of this measurement technique is described elsewhere.[24] Unlike phase contrast imaging which is primarily sensitive to crystalline order, the *Z*-contrast images clearly distinguish, by the degree of brightness, high density HfO_2 from the low density (dark) SiO_2-like interfacial layer (IL) and produce the more accurate layer thickness dimensions, relative to HRTEM, indicated in Table I.[25]

Electrical properties of the dielectric films and interfaces have been characterized by MOSFET measurements. Transistors were fabricated using 3 nm HfO_2 gate dielectric with 10 nm TiN/poly-Si gate electrodes formed by chemical vapor deposition (CVD) of tetrakis(diethylamido)titanium (TDEAT) with NH_3, followed by 180 nm of phosphorus doped poly-Si. The relationship between gate current density J_g at $V_{fb}-1$ (where V_{fb} is the flatband voltage) and EOT for the gate dielectric stacks with several types of bottom interfacial oxides, with and without NH_3 treatment, is illustrated in the plot of Fig. 1(a). For each bottom interfacial oxide studied, incorporating NH_3 resulted in slightly lower EOT relative to the same interfacial oxide without NH_3. This is consistent with the higher permittivity reported for silicon oxynitride relative to SiO_2.[26] The influence of the NH_3 treatment on J_g is more difficult to isolate since leakage current is a strong function of EOT.

Figure 1(b) shows the plot of EOT versus effective high field electron mobility at 1 MV/cm. Formation of quality thermal SiO_2 interface between the Si substrate and high-*k* dielectric enhances electrical performance, specifically, electron mobility.[27] Although a comprehensive discussion of mobility mechanisms is not the focus of this article, there have been numerous reports that identify various specific components of mobility degradation with HfO_2, including phonon scattering,[28] Coulomb scattering,[29] transient charge trapping,[30] and surface roughness.[31] Coulomb scattering has been shown to dominate low field mobility, while phonon

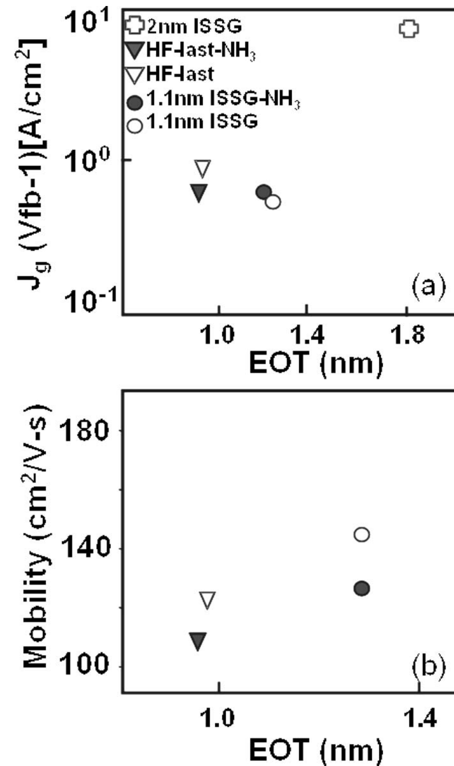

FIG. 1. Plot of (a) gate leakage current J_g vs EOT and (b) high field mobility vs EOT for transistors with 3 nm HfO_2 and several types of bottom interfacial oxides compared with and without NH_3 treatment.

scattering and surface roughness dominate mid and high field mobilities, respectively.[32] Kirsch *et al.* investigated improvements in peak and high field electron mobility corresponding to physical scaling of the HfO_2 layer and attributed the results to reduced charge trapping and Coulomb scattering in thinner films.[33] The general trend of mobility degradation with aggressive scaling of the bottom interface thickness is observed in Fig. 1(b), where an HF-last chemically treated Si substrate is compared with a 1.1 nm thick ISSG SiO_2 interface, with and without NH_3. Mobility degradation associated with the NH_3 treated interfacial oxides may correspond to a combination of nonstoichiometric SiO_2 and the remote Coulomb scattering (RCS) contribution from the HfO_2 film in closer proximity to the substrate.

The chemical state of elements in the transition region between substrate Si and HfO_2 strongly influences device performance parameters such as gate leakage current, electron and hole trapping characteristics, and electron mobility across the channel. Therefore, it is critical to distinguish interfacial microroughness originating from nonuniform protrusion of crystalline HfO_2 grains into the underlying, low density, amorphous SiO_2 layer from chemical intermixing corresponding to Hf silicate ($HfSiO_x$) formation. Since both scenarios are characterized by an (intermediate) electron density between stoichiometric SiO_2 and HfO_2, the core level binding energies of the samples were measured by high resolution XPS at the National Synchrotron Light Source (NSLS) at Brookhaven National Laboratory on the National Institute of Standards and Technology (NIST) beamline X24A. A fixed-exit, double-crystal monochrometer operating

Downloaded 27 May 2008 to 129.6.180.72. Redistribution subject to AIP license or copyright; see http://jap.aip.org/jap/copyright.jsp

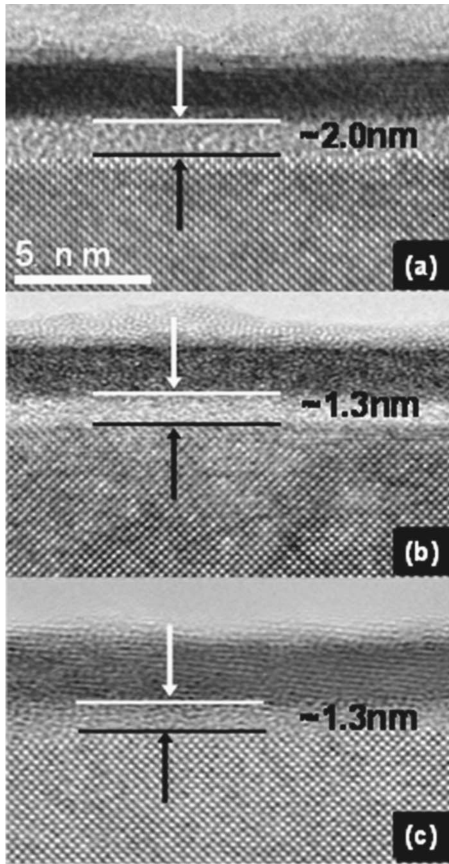

FIG. 2. HRTEM cross-section images of 3 nm HfO_2/Si samples illustrate the dimension of the amorphous interfacial layer (IL) for (a) 2 nm SiO_2, (b) HF-last+NH_3 pre-HfO_2-deposition anneal, and (c) HF-last+NH_3 pre- and post-HfO_2-deposition anneal treatments.

with Si (111) crystals provided photons in the energy range of 2.1–5 keV. Variable kinetic energy x-ray photoelectron spectroscopy (VKE-XPS) measurements were performed with a hemispherical electron analyzer housed in a standard ultrahigh vacuum chamber. Core level spectra recorded at varying kinetic energies enabled chemical depth profiling through the SiO_2 interfacial layer. Additionally, spectra recorded at different electron take-off angles enabled depth sensitive probing of the exposed outer surface of the HfO_2 layer, through the bulk hafnia, to the buried interface.

III. RESULTS AND DISCUSSION

A. Cross-section analysis

The HRTEM micrographs of samples A, B, and C depicted in Fig. 2 illustrate the IL thicknesses of approximately 2.0, 1.3, and 1.3 nm, respectively. The IL is the region formed between the HfO_2 film and the Si substrate. The HAADF-STEM Z-contrast images of the same sample pieces appear in the top portions of Fig. 3 for each sample. The intensities in a Z-contrast image are roughly proportional to the atomic number of the atomic species squared, and the images are therefore dominated by Hf ($Z=72$) that appears white. Element profiles are plotted in the lower portion of the figure and were acquired for each sample along a straight line from the Si substrate through the IL and through the uncapped HfO_2 layer. They were produced by integrating the background corrected EELS intensity (N K, Si K, Hf L, and O K edges) of each element. The position of each profile is aligned to the width of the corresponding STEM image above. They have not been corrected for differences in scattering cross section or sample thickness variations, and their detection sensitivity, which may be influenced by local composition due to scattering of incident electrons and associated signal interference, is on the order of a few at. %.

The influence of the starting Si substrate chemical treatment is clearly indicated by the position and relative intensity of the N profile of each sample, as described previously.[34] The O, N, and Si intensities overlap in sample A at the beginning of the IL, which is consistent with the spectra of SiO_xN_y formation. In contrast, the onset of the N intensity precedes the O intensity profile in the NH_3 pretreated samples B and C and this narrow O-free region is consistent with substrate Si–N bond formation. Medium energy ion scattering (MEIS) was utilized to characterize interfaces representative of samples B and C, and a model consisting of 0.5 nm Si_3N_4 formed on Si gave a good representation of the data.

The element profiles in Fig. 3 also indicate a Hf-free region near the substrate of each sample (the Si/IL region). This observation is supported by the fact that the EELS is more sensitive to high Z elements in a mixed density medium, and significant elastic scattering from the heavy Hf atoms attenuates the low Z oxygen and nitrogen signals. Ni-

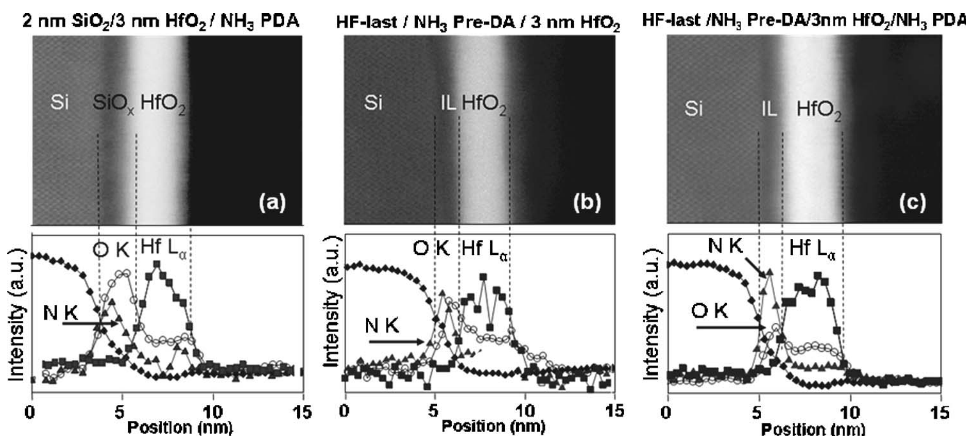

FIG. 3. HAADF-STEM Z-contrast images with element profiles showing changes in the integrated intensities from EELS and EDXS. Data were recorded for a series of points across the gate stack of 3 nm HfO_2 films illustrating relative N incorporation as a function of NH_3 processing for samples (a) A, (b) B, and (c) C as specified in Table I.

Downloaded 27 May 2008 to 129.6.180.72. Redistribution subject to AIP license or copyright; see http://jap.aip.org/jap/copyright.jsp

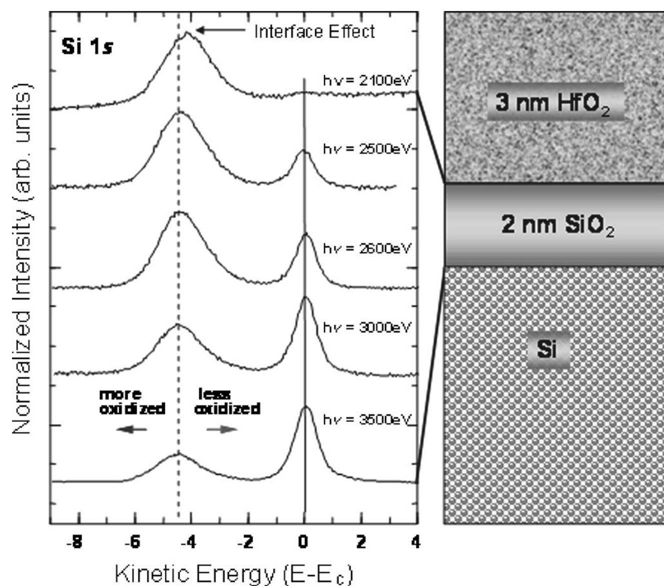

FIG. 4. Si 1*s* spectra from sample A recorded with variable kinetic energy XPS illustrate the region of depth profiling sensitivity and an interface effect near HfO_2.

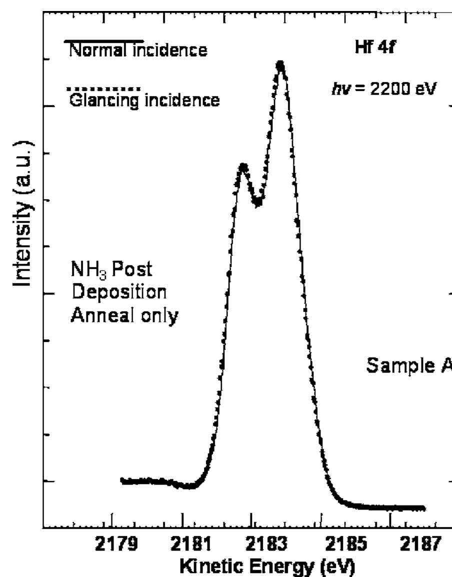

FIG. 5. Hf 4*f* spin-orbit doublet spectra of sample A recorded with photon energy $h\nu$=2200 eV. The lineshape of the Hf 4*f* core level is the same at both glancing and normal photon incident angles, indicating the uniformity of the Hf–N bonding throughout the film.

trogen fully penetrates the HfO_2 layer and accumulates in the Si/IL region of sample A that was subjected only to nitrogen during the NH_3 postdeposition anneal.

B. Depth profiling

Figure 4 demonstrates the Si depth-resolution sensitivity through the thin IL using Si 1*s* VKE-XPS for sample A recorded over the photon energy range 2100 eV$\leqslant h\nu \leqslant$3500 eV. The intensity of the Si 1*s* spectrum at the Si/SiO_2 interface recorded at $h\nu$=3500 eV photon energy is dominated by the substrate (Si^0) signal. Correspondingly, at the low photon energy, $h\nu$=2100 eV, few substrate Si–Si bonds (Si^0) are detected, and the spectrum consists primarily of oxidized Si at the HfO_2/SiO_2 interface. Based on the Si^{4+} peak shift to lower binding energy with decreasing photon energy [Si^{4+} is the standard Si state synonymous in binding energy (BE) with SiO_2], it appears that the Si in the IL is less oxidized closest to the HfO_2 layer following NH_3 PDA. This is because lower kinetic energy electrons probe less of the IL region while favoring the HfO_2 surface. Although this shift may be consistent with Hf silicate formation, it is not thermodynamically favorable for HfO_2 to mix with SiO_2 during thermal processing. It has been shown that various compositions of Hf silicate films demix and form HfO_2 grains embedded in amorphous SiO_2 upon exposure to anneal processing sufficient to induce crystallization.[35–37]

The 3 nm thick HfO_2 layer is too thin for effective VKE-XPS depth profiling at these photon energies using the low binding energy Hf 4*f* core line. Therefore, in order to address the unlikely possibility of Hf silicate formation at the SiO_2/HfO_2 interface, Hf 4*f* spectra were recorded at different electron take-off angles for sample A at $h\nu$=2200 eV. Figure 5 shows spectra which were recorded at interface-sensitive glancing (5°)-photon incidence/normal-electron take-off angle and surface-sensitive normal (80°)-photon incidence/glancing-electron take-off angle. At normal incidence the path of the ejected photoelectrons through the HfO_2 film is increased by approximately a factor of 4 relative to the spectra recorded at glancing incidence. As the escape depth of 2200 eV electrons traveling through HfO_2 is estimated to be ~1.6 nm, this increase in path length would effectively eliminate any interfacial signal arising from the IL. Therefore, these data suggest that the chemical composition around the Hf atoms is uniform throughout the film, and there is little if any detectable change in Hf bonding at the IL relative to the outer surface. The data are therefore consistent with no Hf silicate formation at the interface, for Hf silicate would have a significant Hf 4*f* core level binding energy shift to higher energy relative to the HfO_2.[38] Additionally, because a corresponding change in the Hf 4*f* line shape does not accompany the "interface effect" observed in the Si 1*s* spectra of sample A in Fig. 4, it is clear that Hf has scavenged O and reduced the Si–O coordination near the HfO_2/Si interface. This conclusion is consistent with the mechanistic pathways proposed for electrical performance of advanced MOSFET devices described previously.[39]

The change in chemical bonding of the Si in the IL was also examined by recording high resolution Si 2*p* spectra at $h\nu$=2200 eV for samples A, B, and C. These spectra are shown in Fig. 6 and normalized to the Si^0 intensity. Recall that N is observed in the elemental profiles of sample A (Fig. 3) near the bottom interface due to the NH_3 PDA process; however, the XPS spectra for this sample shown in Fig. 6 exhibit a Si^{4+} peak similar to fully oxidized thermal SiO_2. Samples B and C, however, which were exposed to NH_3 processing pre-HfO_2-deposition (and are consistent with Si_3N_4 at the interface from MEIS data), do not exhibit Si^{4+}, rather, these spectra suggest the corresponding IL may consist of Si–N bonds where N and/or NH has exchanged for O. The resultant SiO_xN_y layer remains amorphous as illustrated in the HRTEM image of Fig. 2, and there is little evidence of Si fourfold coordination with O.

Downloaded 27 May 2008 to 129.6.180.72. Redistribution subject to AIP license or copyright; see http://jap.aip.org/jap/copyright.jsp

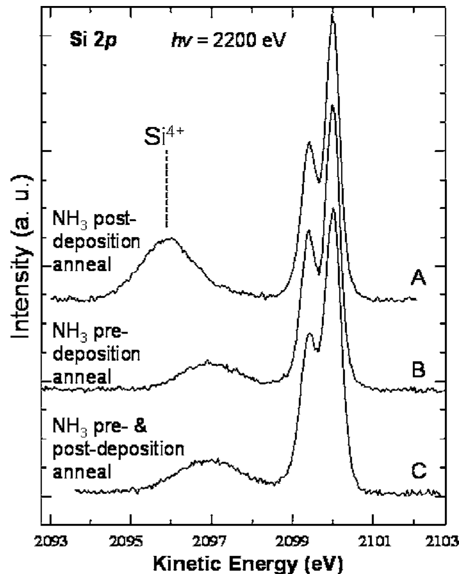

FIG. 6. Si $2p$ spectra recorded at $h\nu$=2200 eV illustrating the binding energy difference in the Si^{4+} peak signal between the thermal oxide interface of sample A, the HF-last+NH_3 pre-HfO_2-deposition anneal treatment of sample B, and the HF-last+NH_3 pre- and post-HfO_2-deposition anneal treatment of sample C.

C. Hf and N core level spectra

The Hf $4f$ core level spectra of the sample set illustrated in Fig. 7 clearly indicate the influence of the NH_3 PDA on the local coordination of the Hf atoms. The narrow line shape of the Hf core level spectrum of sample B is identical to that measured (not shown) from an as deposited HfO_2 film that serves as a reference standard. In order to construct the line shape parameters to decompose the more complicated spectra of samples A and C, this spectrum was fitted with a single Hf $4f$ doublet as shown (the dots are the measured data points and the solid line is the fit). The line shape parameters obtained utilizing a Shirley background are spin-orbit splitting of 1.66 eV, $4f_{7/2}$ to $4f_{5/2}$ branching ratio of 1.31, Lorentzian width of 0.17 eV, and Gaussian width of 1.0 eV. This branching ratio is close to the statistical $2J+1/2J+1$ value of 1.33 for the $J=7/2$ and 5/2 components, although both the Lorentzian and Gaussian widths are much larger than expected and may be attributed to charge fluctuations in the amorphous HfO_2.[40] These line shape fitting parameters were then applied[41] to the core level spectra of the NH_3 PDA samples, A and C, shown in Fig. 7, where the spectra were recorded at the more interface-sensitive glancing-photon incidence/normal-electron take-off angle. Clearly, the effect of N substitution for O around the Hf manifests itself as a distinct Hf core level shift to lower binding energy due to the reduced electronegativity of N relative to O. The arrows in Fig. 7 indicate the appearance of the Hf–N bond component which further broadens the Hf $4f$ linewidth. This result is consistent with the analysis of similar samples exposed to NH_3 PDA by Lee *et al.*[42] in that Hf–N bonding results in a shift to lower binding energy for the Hf $4f$ doublet. Sample C exhibits additional peak broadening over sample A due to the increased Hf—N bond formation from the NH_3 pre-DA. NH_3 nitridation of the substrate prior to HfO_2 deposition results in N redistribution from the bottom interface to the HfO_2 film during the NH_3 PDA. Therefore, sample C experiences nitrogen exposure from two (sources) sides during the PDA process, that sample B did not receive, which is revealed by the core level decomposition and is consistent with the measured total N dose. The total N dose (see Table I) for sample C is 5.91×10^{15} atoms/cm^2, which is $\sim$1.7 times greater than the N dose of sample A and $\sim$2.8 times greater than the N dose of sample B. The N dose difference between samples B and C is attributed to the NH_3 PDA.

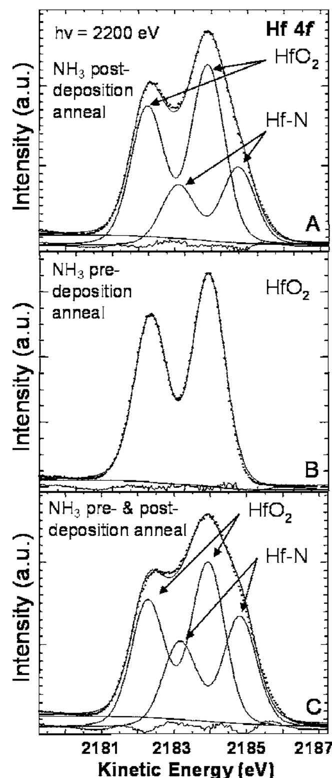

FIG. 7. Hf $4f$ spin-orbit doublet spectra of samples A, B, and C recorded at $h\nu$=2200 eV. The spectrum of sample B (as deposited) is identical to the Hf $4f$ spectrum of a reference HfO_2 film. Samples A and C exhibit line shape broadening due to the incorporation of N (Hf–N bonding) arising from the NH_3 post-HfO_2-deposition anneal.

The N $1s$ spectra measured for the three-sample set are illustrated in Fig. 8. Sample A was (only) exposed to the NH_3 postdeposition process, and it appears to exhibit Hf–N bonds with no appreciable Si–N bonding, although the elemental profile data (Fig. 3) for this sample do indicate N in the IL. Sample B was (only) exposed to the NH_3 predeposition process, and Hf–N bonding is not observed in the N $1s$ spectrum from this sample. Sample C exhibits a N $1s$ spectrum that is comprised of both components: the Si–N peak corresponding to the NH_3 predeposition anneal process and the Hf–N peak resulting from the NH_3 postdeposition anneal process.

D. N exchange for O

Although nitridation of HfO_2 increases the barrier for oxygen and boron diffusion,[43] introducing N adds electrically active states above the valence band, which lowers the valence band offset and thereby reduces the band gap in

Downloaded 27 May 2008 to 129.6.180.72. Redistribution subject to AIP license or copyright; see http://jap.aip.org/jap/copyright.jsp

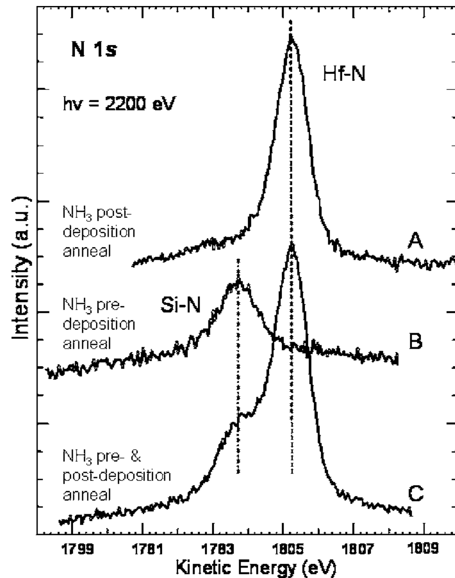

FIG. 8. N 1s core level spectra for samples A, B, and C recorded at $h\nu$ =2200 eV. The spectrum from sample C is closely modeled by the sum of the spectra from samples A and B.

HfO_2. This change in electronic structure is a direct reflection of the lower atomic number and hence less tightly bound valence 2p orbitals of N relative to O. Substitution of N for O in the unit cell leads to a hole in the valence band (p-type material) and favors anion vacancy formation.[44] A direct comparison of the valence band measurement of samples A, B, and C by XPS (measured by Charles Evans and Associates using Al $K\alpha$ source) is shown in Fig. 9. Samples A and C reveal an increase in the valence band maximum (VBM) that trends with the N dose (see Table I) from the NH_3 anneal process: as the N concentration increases, more N 2p states extend toward the conduction band, resulting in the reduction of the band gap. The VBM consists mainly of O 2p-like nonbonding orbitals of π symmetry, while the conduction band minimum (CBM) is due to Hf 5d nonbonding states.[45] As a result, the band gap of HfO_xN_y is set primarily by atomic energies, and adding N reduces the band gap by raising the VBM. It is proposed that NH_3 dissociates to NH species which exchange for O during the PDA process, since

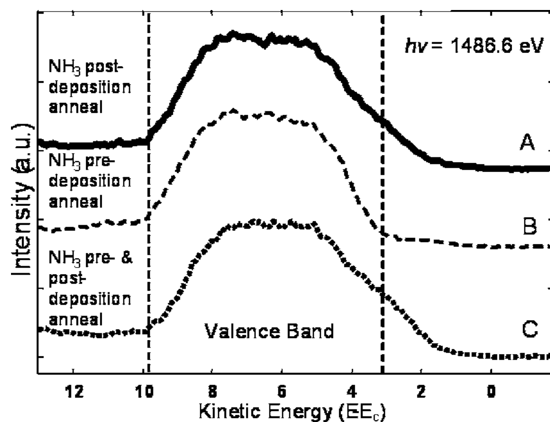

FIG. 9. Valence band measurements of samples A, B, and C recorded at $h\nu$=1486.6 eV illustrating the increase in the valence band maximum associated with N incorporation in HfO_2.

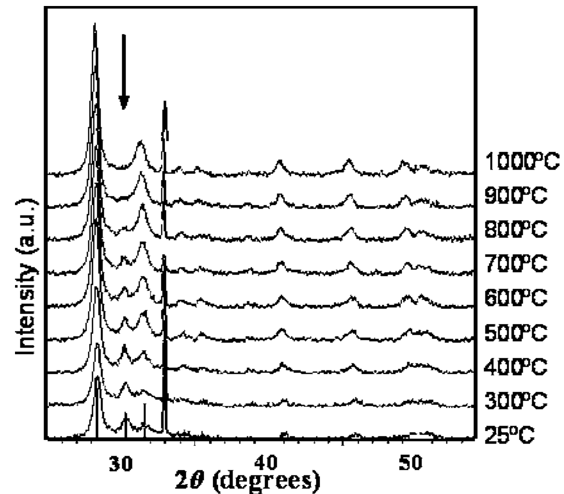

FIG. 10. GIXRD 2θ patterns from a HfO_2 film annealed at 100 °C increments. The feature at 2θ~30.4° indicates a transition (from orthorhombic or tetragonal) to m-HfO_2 above 800 °C.

the electron configuration of NH=O=$1s^2 2s^2 p^4$, and isoelectronic species are expected to exhibit similar chemical and physical characteristics.

E. Crystalline structure analysis

Thin as deposited hafnia films have been reported to exhibit a phase change following exposure to anneal temperature $\geqslant$500 °C.[46] The films are typically amorphous or nanocrystalline when deposited at 330 °C and become polycrystalline, largely in the monoclinic phase with a smaller fraction of tetragonal and/or orthorhombic phase detected in films annealed up to the 700 °C PDA temperature.[47] This phase transition is clearly illustrated in the GIXRD 2θ patterns of Fig. 10 which were obtained for a single 4 nm HfO_2 sample measured at 100 °C increments in N_2 ambient. The arrow in Fig. 10 points to the feature at 2θ~30.4° which appears most prominently at 400 °C and diminishes completely above 800 °C where the diffraction spectrum matches monoclinic HfO_2 (m-HfO_2). This transitional peak corresponds to either the orthorhombic or tetragonal phase of HfO_2; it may also signify the coexistence of both phases. Specific identification is hampered by the near coincidence of features from both phases at that position as identified in the International Centre for Diffraction Data (ICDD) powder diffraction card files.[48]

In order to investigate the chemical effect of N incorporation on the crystallization kinetics of HfO_2, an additional set of samples, consisting of 4 nm thick HfO_2 deposited on 1 nm SiO_2/Si(100), has been annealed in N_2 and NH_3 ambients for x-ray diffraction comparison. The GIXRD patterns corresponding to N_2 and NH_3 PDA processing at 700 °C are illustrated in Figs. 11(a) and 11(b), respectively; they are plotted on a scale different from Fig. 10. The sample in Fig. 11(a) is representative of the thermal response of HfO_2 (no NH_3 reaction) and therefore provides a reference for identifying differences due to N incorporation during NH_3 PDA. The sample measured in Fig. 11(b) is identical to sample A (discussed previously), with the exception of having a 1 nm SiO_2 interface layer. The prominence of the peak at 2θ

Downloaded 27 May 2008 to 129.6.180.72. Redistribution subject to AIP license or copyright; see http://jap.aip.org/jap/copyright.jsp

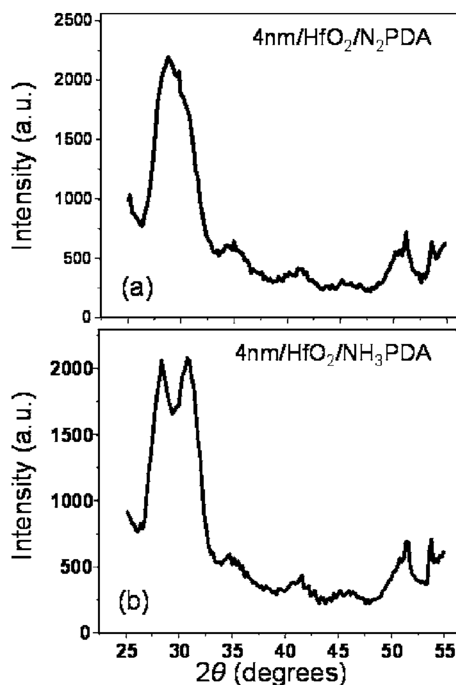

FIG. 11. GIXRD 2θ patterns for 4 nm HfO_2 films illustrating the structural difference between (a) the reference thermal response from the N_2 PDA and (b) the effect of N incorporation from the NH_3 PDA.

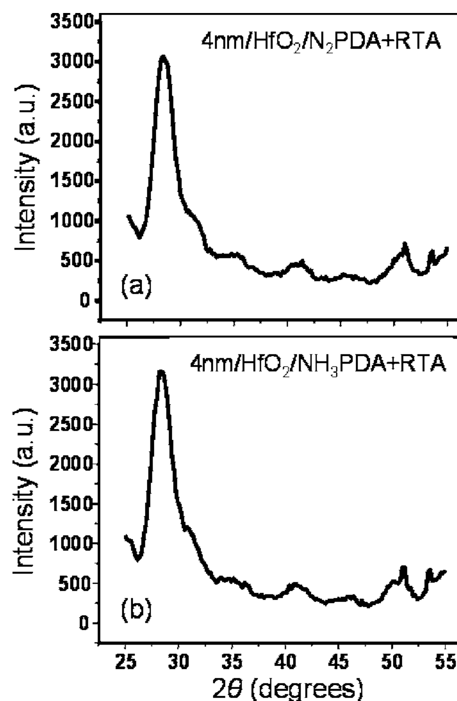

FIG. 12. GIXRD 2θ patterns illustrating the m-HfO_2 phase for 4 nm HfO_2 films exposed to (a) N_2 PDA plus N_2 RTA and (b) NH_3 PDA plus N_2 RTA.

$\sim$30.4° in Fig. 11(b) relative to the thermal response pattern of Fig. 11(a) is due to the substitution of NH for O in the unit cell structure, upon NH_3 reaction, as detected by XPS (Fig. 7). This peak may be indicative of the tetragonal or orthorhombic phase (or both) of HfO_2, originating from a change in bond lengths or bond angles, respectively, relative to m-HfO_2.

It has been shown that Hf–N bonds produced in reactively sputtered (Hf target in $Ar/N_2/O_2$ mixed ambient) HfO_xN_y films are not stable during subsequent anneal cycles due to the substitutional characteristics of oxygen, resulting in significant loss of nitrogen from the bulk films.[49,50] Since these films are being investigated for transistor gate dielectric applications, the thermal stability must be evaluated with respect to the source/drain implant dopant activation anneal process. Therefore, in addition to comparing the influence of the ambient (NH_3 versus N_2) during the (intermediate) 700 °C/60 s PDA process, a subset of samples has also been subjected to the 1000 °C/10 s RTA process in N_2 ambient. As indicated in the GIXRD patterns of Figs. 12(a) and 12(b), both films consist of m-HfO_2, and there is no apparent structural dependence on the intermediate PDA ambient. Exposure to the RTA process is sufficient to cause further dissociation of NH to N+H where H outdiffusion results in atomic N exchange for O. Concern that N outdiffusion and O_2 indiffusion may be exacerbated in uncapped blanket films during RTA (the dielectric is capped by the electrode layer in standard device processing) was addressed by analyzing HAADF-STEM images and element profiles (not shown) of a sample identical to that of Fig. 12(b), but capped with 10 nm TiN prior to RTA. The relative N content ([N]/[O]+[N]) in the SiO_xN_y IL, estimated at $\sim$10 at. %, was found to be very similar to that of the uncapped sample of Fig. 12(b). Following TiN etch, XRD patterns of this film also correspond to m-HfO_2. The significant [N] detected in the IL of the capped sample following RTA, coupled with the resultant m-HfO_2 phase, support the proposal that the RTA cycle dissociates the NH molecule, which liberates hydrogen and results in atomic N exchange for O in m-HfO_2.

IV. CONCLUSION

Thin HfO_2 blanket films have been deposited on chemically prepared (p-type) Si (100) substrates to produce $HfO_2/SiO_2/Si$ samples which have been alternately exposed to anneal cycles in NH_3 and N_2 ambients for direct comparison. HAADF-STEM Z-contrast images with element profiles showing changes in the integrated intensities from EELS and EDXS data recorded for a series of points across the gate stack of 3 nm HfO_2 films have been correlated with synchrotron XPS Si 2p and N 1s spectra to identify substrate Si–N bond formation associated with HF-last+NH_3 substrate treatments. The NH_3 anneal ambient has been shown to produce Hf–N bond formation and influence the crystallographic microstructure of thin HfO_2 films. The Si 1s spectra obtained with VKE-XPS, however, reveal a shift to higher binding energy of the Si^{4+} peak at the HfO_2/SiO_2 interface with increasing photon energy, while the Hf 4f core level spectra, obtained over a wide range of incident angles, exhibited no observable change in binding energy or line shape. It is difficult to distinguish chemical intermixing corresponding to Hf silicate formation from microroughness of the crystalline-amorphous interface, since both conditions are characterized as a transition region of intermediate electron density between stoichiometric amorphous SiO_2 and crystalline HfO_2. However, using the combination of the Si 1s spectra recorded via VKE-XPS depth profiling and the Hf 4f

Downloaded 27 May 2008 to 129.6.180.72. Redistribution subject to AIP license or copyright; see http://jap.aip.org/jap/copyright.jsp

spectra recorded at different electron take-off angles (at $h\nu = 2200$ eV) shows that the N content and chemistry in the HfO_2 film are uniform throughout the thickness of the film and that the underlying SiO_2 becomes O deficient in contact with HfO_2.

For HfO_2/SiO_2 thin film systems exposed to the NH_3 PDA process, the Hf–N bonding component detected in the Hf 4*f* XPS spectra has been correlated with a transitional phase peak at $2\theta \sim 30.4°$ in GIXRD patterns. During the 700 °C/60 s NH_3 exposure, it is proposed that the NH molecule exchanges for O, since similar chemical and physical properties are expected for these isoelectronic species. Following RTA in N_2 ambient, samples previously exposed to NH_3 or N_2 PDA, either uncapped or capped with TiN, produce GIXRD 2θ patterns consistent with *m*-HfO_2. Since the at. % N remains essentially unchanged in the capped and uncapped NH_3 PDA films following RTA and both transition to *m*-HfO_2, it is not expected that N outdiffusion or O_2 indiffusion appreciably influences the measured response. Rather, the RTA process gives rise to further dissociation of the NH molecule, which is accompanied by the liberation of hydrogen resulting in atomic N exchange for O in the *m*-HfO_2 cell structure.

ACKNOWLEDGMENTS

The authors express their appreciation to W. N. Lennard at the University of Western Ontario for NRA measurements, T. Gustafsson and E. Garfunkel at Rutgers University for MEIS measurements, and E. Watkins at the Los Alamos Neutron Science Center for GIXRD measurements. Use of the National Synchrotron Light Source, Brookhaven National Laboratory, was supported by the U.S. Department of Energy, Office of Science, Office of Basic Energy Sciences, under Contract No. DE-AC02-98CH10886.

[1]International Technology Roadmap for Semiconductors, 2003, pp. 35–37.
[2]G. D. Wilk, R. M. Wallace, and J. M. Anthony, J. Appl. Phys. **89**, 5243 (2001).
[3]M. R. Visokay, J. J. Chambers, A. L. P. Rotondaro, A. Shanware, and L. Colombo, Appl. Phys. Lett. **80**, 3183 (2002).
[4]M. A. Quevedo-Lopez *et al.*, Appl. Phys. Lett. **81**, 1074 (2002).
[5]C. H. Choi, T. S. Jeon, R. Clark, and D. L. Kwong, IEEE Electron Device Lett. **24**, 215 (2003).
[6]J. Barnett, N. Moumen, J. J. Peterson, P. Kirsch, A. Neugroschel, G. Bersuker, and H. Huff, Electrochem. Trans. **1**, 43 (2005).
[7]G. Bersuker, P. M. Zeitzoff, J. Barnett, N. Moumen, B. Foran, C. D. Young, J. Peterson, and P. Lysaght, Jpn. J. Appl. Phys., Part 1 **43**, 7899 (2004).
[8]S. Stemmer, Z. Chen, C. G. Levi, P. Lysaght, B. Foran, J. A. Gisby, and J. R. Taylor, Jpn. J. Appl. Phys., Part 1 **42**, 3593 (2003).
[9]C. S. Kang *et al.*, Appl. Phys. Lett. **81**, 2593 (2002).
[10]G. Shang, P. W. Peacock, and J. Robertson, Appl. Phys. Lett. **84**, 106 (2004).
[11]R. G. Forbes, Ultramicroscopy **89**, 7 (2001).
[12]R. G. Forbes, Solid-State Electron. **45**, 779 (2001).
[13]H. O. Pierson, *Handbook of Refractory Carbide and Nitride* (Noyes, Park Ridge, NJ, 1996).
[14]E. C. Lee and K. J. Chang, Phys. Rev. B **66**, 233205 (2002).
[15]N. S. Saks and D. I. Ma, Appl. Phys. Lett. **67**, 374 (1995).
[16]N. S. Saks and J. M. Andrews, J. Electron. Mater. **21**, 775 (1992).
[17]F. Bozso and P. Avouris, Phys. Rev. Lett. **57**, 1185 (1986).
[18]R. J. Hamers, P. Avouris, and F. Bozso, Phys. Rev. Lett. **59**, 2071 (1987).
[19]M. J. Dresser, P. A. Taylor, R. M. Wallace, W. J. Choyke, and J. T. Yates, Surf. Sci. **218**, 75 (1989).
[20]N. Franco *et al.*, Phys. Rev. Lett. **79**, 673 (1997).
[21]L. Kubler, J. L. Bischoff, and D. Belmont, Phys. Rev. B **38**, 13113 (1988).
[22]K. T. Queeney, Y. J. Chabal, and K. Raghavachari, Phys. Rev. Lett. **86**, 1046 (2001).
[23]J. L. Gavartin, A. L. Shluger, A. S. Foster, and G. I. Bersuker, J. Appl. Phys. **97**, 53704 (2005).
[24]B. Foran, J. Barnett, P. S. Lysaght, M. P. Agustin, and S. Stemmer, J. Electron Spectrosc. Relat. Phenom. **143**, 149 (2005).
[25]A. C. Diebold, B. Foran, C. Kisielowski, D. A. Muller, S. J. Pennycook, E. Principe, and S. Stemmer, Microsc. Microanal. **9**, 493 (2003).
[26]M. L. Green, E. P. Gusev, R. Degraeve, and E. L. Garfunkel, J. Appl. Phys. **90**, 2057 (2001).
[27]J. Barnett *et al.*, Mater. Res. Soc. Symp. Proc. **811**, E1.4 (2004).
[28]M. V. Fischetti, D. A. Neumayer, and E. A. Cartier, J. Appl. Phys. **90**, 4587 (2001).
[29]M. Hiratani, S. Saito, Y. Shimamoto, and K. Torii, Jpn. J. Appl. Phys., Part 1 **41**, 4521 (2002).
[30]H. Lee, Tech. Dig. - Int. Electron Devices Meet. **2004**, 859.
[31]S. Saito, D. Hisamoto, S. Kimura, and H. Hiratani, Tech. Dig. - Int. Electron Devices Meet. **2003**, 797.
[32]S. Takagi, A. Toriuni, M. Iwase, and H. Tango, IEEE Trans. Electron Devices **41**, 2357 (1994).
[33]P. D. Kirsch *et al.*, J. Appl. Phys. **99**, 023508 (2006).
[34]P. S. Lysaght, B. Foran, G. Bersuker, J. J. Peterson, C. D. Young, P. Majhi, B.-H. Lee, and H. R. Huff, Appl. Phys. Lett. **87**, 082903 (2005).
[35]H. Kim and P. C. McIntyre, J. Appl. Phys. **92**, 5094 (2002).
[36]S. Ramanathan, P. C. McIntyre, J. Luning, P. S. Lysaght, Y. Yang, Z. Chen, and S. Stemmer, J. Electrochem. Soc. **150**, F173 (2003).
[37]S. Stemmer, Y. Li, B. Foran, P. S. Lysaght, S. K. Streiffer, P. Fuoss, and S. Seifert, Appl. Phys. Lett. **83**, 3141 (2003).
[38]P. D. Kirsch, C. S. Kang, J. Lozano, J. C. Lee, and J. G. Ekerdt, J. Appl. Phys. **91**, 4353 (2002).
[39]G. Bersuker, J. Peterson, J. Barnett, J. Sim, R. Choi, B. H. Lee, P. Lysaght, and H. R. Huff, J. Electrochem. Soc. **501**, 623 (2006).
[40]J. C. Woicik and P. Pianetta, in *Synchrotron Radiation Research: Advances in Surface and Interface Science: Issues and Technology*, edited by R. Z. Bachrach (Plenum, New York, 1992).
[41]J. C. Woicik, P. Pianetta, and T. Kendelewicz, Phys. Rev. B **40**, 12463 (1989).
[42]M. Lee, Z.-H. Lu, W.-T. Ng, D. Landheer, X. Wu, and S. Moisa, Appl. Phys. Lett. **83**, 2638 (2003).
[43]H. J. Cho, C. S. Kang, K. Onishi, S. Gopalan, R. Nieh, S. Krishnan, and J. C. Lee, IEEE Electron Device Lett. **23**, 249 (2002).
[44]J. Robertson, Philos. Mag. B **62**, 47 (1991).
[45]S. Sayan *et al.*, J. Appl. Phys. **96**, 7485 (2004).
[46]P. S. Lysaght, P. J. Chen, R. Bergmann, T. Messina, R. W. Murto, and H. R. Huff, J. Non-Cryst. Solids **303**, 54 (2002).
[47]N. V. Nguyen, A. V. Davydov, D. Chandler-Horowitz, and M. M. Frank, Appl. Phys. Lett. **87**, 192903-1 (2005).
[48]M.-Y. Ho *et al.*, J. Appl. Phys. **93**, 1477 (2003).
[49]C. H. Choi, J. S. Rhee, T. S. Jeon, N. Lu, J. H. Sim, R. Clark, M. Niwa, and D. L. Kwong, Tech. Dig. - Int. Electron Devices Meet. **2002**, 857.
[50]J. F. Kang *et al.*, Appl. Phys. Lett. **84**, 1588 (2004).

Downloaded 27 May 2008 to 129.6.180.72. Redistribution subject to AIP license or copyright; see http://jap.aip.org/jap/copyright.jsp